Fusion Engineering and Design 83 (2008) 1335–1339

Contents lists available at ScienceDirect

Fusion Engineering and Design

journal homepage: www.elsevier.com/locate/fusengdes

MHD simulations of liquid metal flow through a toroidally oriented manifold

N.B. Morley[a,*], M.-J. Ni[a], R. Munipalli[b], P. Huang[b], M.A. Abdou[a]

[a] Mechanical and Aerospace Engineering, University of California, Los Angeles, CA 90095, USA
[b] Hypercomp, Inc., 2629 Townsgate Rd. Suite 105, Thousand Oaks, CA 91361, USA

ARTICLE INFO

Article history:
Available online 20 June 2008

Keywords:
Liquid metal blankets
Magnetohydrodynamics (MHD)
Fusion
Manifold
Flow balance
Computational fluid dynamics (CFD)

ABSTRACT

In fusion liquid metal (LM) blankets, magnetohydrodynamic (MHD) effects will dominate the pressure drop and velocity profiles of the liquid metal flow, including the manifold regions needed to distribute flow. However, there is very little experimental data available for manifolds with geometry and orientation to the magnetic field similar to typical dual-coolant lead–lithium (DCLL) blanket designs—and the data that does exist indicates strong non-uniformity of flow partitioning between parallel channels can occur. In order to begin to address these issues for the US DCLL blanket design, a series of 3D MHD simulations has been performed at relevant magnetic interaction parameters. The geometry considered has a single rectangular supply channel entering a rectangular expansion with toroidal field oriented along the expansion direction, finally feeding into 3 rectangular parallel channels stacked in the field direction. These simulations match the range of experimental conditions achievable in a concurrent experimental test campaign. Various conditions of flowrate and field strength are explored. The MHD effects generally act to make the flow distribution more uniform than without a field. However flow imbalances as great as 26% from uniform are seen under the conditions analyzed.

1. Introduction

A key feature of liquid metal (LM) breeding blankets is the liquid metal flow manifold, which must distribute/collect the liquid metal coolant to/from parallel blanket channels. The dual-coolant lead–lithium (DCLL) blanket concept, as currently envisioned in the US [1,2], has several poloidally running, toroidally stacked, parallel channels. The blanket requires a manifold section to accept liquid lead–lithium from a central supply, distribute it toroidally, and then feed it into the poloidally running parallel channels. A similar manifold is required at the end of the parallel channel runs to collect the lead–lithium and merge the flows into a central return line. Examples of such manifolds and their orientations can be seen in Fig. 1, representative of the US DCLL test blanket module design.

These manifolds can have a non-negligible effect on the total pressure drop of the system, and can strongly influence the uniformity of flow distribution between the multiple parallel channels. This later effect, in particular, is of critical concern for the operation of the blanket in order to prevent unacceptable overheating of parallel channels with reduced flow. To investigate flow in the DCLL manifolds, both numerical simulations and experimental investigation are underway at UCLA. Table 1 provides quantification of the relative sizes, flow conditions, and scaling parameters for DCLL Pb–17Li manifolds. Reported here are first results of 3D MHD numerical simulations of LM flow through a geometrically idealized manifold with size and scaling parameters in the range of the experimental apparatus.

2. Description of numerical simulations

The simulation of LM-MHD flowing at high Hartmann numbers has been a topic of great interest in the development of a fusion reactor blanket. The flow is governed by the following Navier–Stokes equation and continuity equation, which represent the conservation of momentum and mass:

$$\frac{1}{N}\left(\frac{\partial u}{\partial t} + u \cdot \nabla u\right) = -\nabla p + \frac{1}{Ha^2}\nabla^2 u + (J \times B) \tag{1}$$

$$\nabla \cdot u = 0 \tag{2}$$

where u and p are the non-dimensional velocity vector and pressure scaled with u_0 and $\sigma u_0 B^2 L$, respectively. With L defined as a characteristic length, the Reynolds number is $Re = Lu_0/\nu$, the Hartmann number is $Ha = LB\sqrt{\sigma/\rho\nu}$, and $N = Ha^2/Re$ is the interaction parameter (or Stuart number). The current density, J, scaled by $\sigma u_0 B$, can

* Corresponding author at: 43-133 Engineering IV, Mechanical and Aerospace Engineering, UCLA, Los Angeles, CA 90095-1597, USA. Tel.: +1 310 206 1230; fax: +1 310 825 2599.
E-mail address: morley@fusion.ucla.edu (N.B. Morley).

0920-3796/$ – see front matter © 2008 Elsevier B.V. All rights reserved.
doi:10.1016/j.fusengdes.2008.04.010

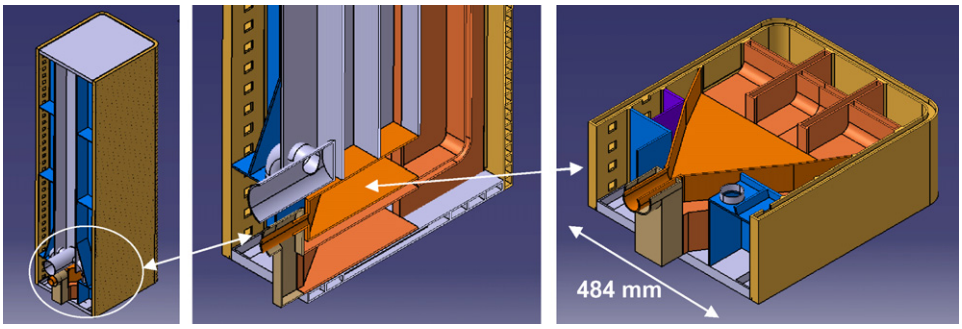

Fig. 1. US DCLL test blanket module: different views of the manifold region.

Table 1
Typical dimensions, flow conditions and scaling parameters for the DCLL manifold regions

	Demo	US-TBM	Experimental
Manifold width, $2a$ (m)	2	0.4	0.1
Manifold height, $2b$ (m)	0.2	0.1	0.02
Manifold axial length, L (m)	0.5	0.2	.05
Number poloidal channels	8	3	3
Average flow velocity (nominal)[a], u_0 (m/s)	0.1	0.08	0.036[b]
Magnetic field (outboard), B (T)	4	4	1.7[c]
Working liquid metal	Pb–Li (550 °C)	Pb–Li (400 °C)	Ga–In–Sn or Hg (RT)
Hartmann number (based on a), $Ha = aB\sqrt{\sigma/\rho\nu}$	10^5	17,000	3000[c]
Reynolds number (based on b), $Re = bu_0/\nu$	10^5	30,000	900[b]
Interaction parameter, $N = Ha^2/Re$	10^5	10^4	10^4[b]
Manifold length ratio, L/a	0.25	1	1

[a] Velocity in the expanded region; inlet channel velocity will be higher.
[b] Adjustable value.
[c] Maximum continuous value.

be determined from Ohm's law:

$$J = -\nabla\varphi + u \times B \tag{3}$$

where φ is the electrical potential scaled by u_0BL. The current density is conservative, such that:

$$\nabla \cdot J = 0 \tag{4}$$

From Eqs. (3) and (4), one can get the electrical potential equation as:

$$\nabla \cdot (\nabla\varphi) = \nabla \cdot (u \times B) \tag{5}$$

In this work, the 3D unsteady MHD code HIMAG with consistent and conservative numerical schemes for determination of current density on a rectangular collocated mesh, is utilized to solve Eqs. (1)–(4). Details of formulation and validation of this code are reported elsewhere [3–5].

The manifold geometry analyzed here, shown in Fig. 2, is identical to the planned experiment given in Table 1. A single rectangular inlet channel undergoes an abrupt 4x expansion, and then subdivides into 3 parallel channels. Table 2 summarizes the parameter space investigated. The $y = 0$ plane is taken as a symmetry plane, and so only half of the geometry as shown in Fig. 2 is meshed. As a rough approximation of flow with insulating flow channel inserts, the analyses utilize electrically insulated walls. Flow is set to 4x u_0 at the inlet, and pressures and normal current density at the outlets of the 3 parallel channels are set to 0. As described in Ref. [6], this outlet

Table 2
Specific flow conditions and physical properties for 3D simulations

	Calculations
u_0 (m/s)	0.01, 0.02
B (T)	1.273–1.8
LM	Ga–In–Sn (RT)
Density, ρ (kg/m^3)	6330[a]
Conductivity, σ ($\times 10^6$ S/m)	3[a]
Viscosity, ν ($\times 10^{-7}$ m^2/s)	4[a]
Ha	2190–3097
Re	215–500
N ($\times 10^4$)	1–3.8

[a] Measured values.

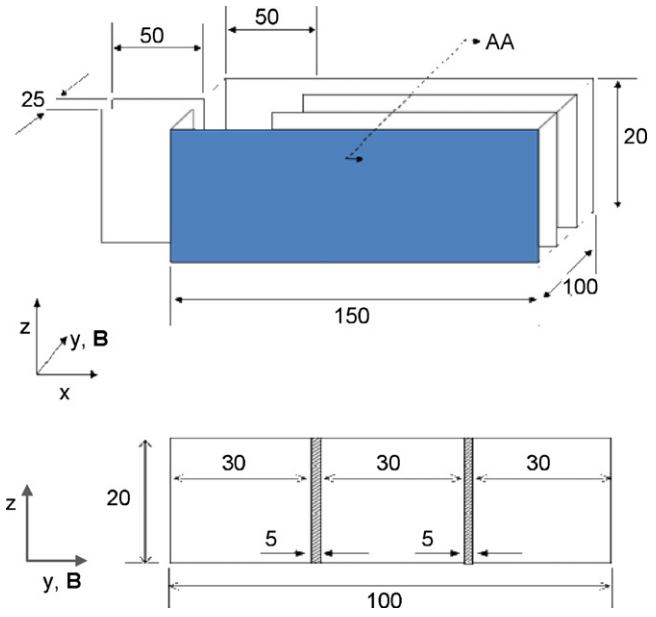

Fig. 2. Geometric model of idealized DCLL manifold used in 3D simulations (dimensions in mm, not to scale).

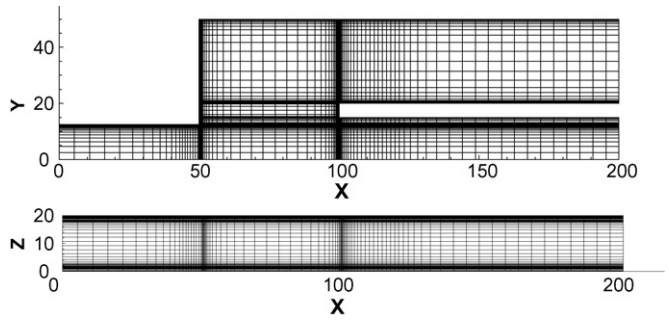

Fig. 3. Computational mesh used for 3D simulations comprising 353,000 cells, with symmetry at the $y = 0$ and $x = 200$ planes (dimensions in mm).

condition is considered as imposing a kind of symmetry, where the 3 channels continue and then enter another manifold where they are consolidated into a return channel—with the same pressure drop behavior as the inlet manifold. Such an assumption appears to be justified when considering a simple expansion/contraction pair according to the high *Ha* and *N* linear theory as discussed in Ref. [7]. However, some remarks on this assumption are made later in Section 5.

A typical mesh for this analysis is shown in Fig. 3, where dividing walls are not explicitly modeled. HIMAG computational runs are executed on a parallel linux cluster using typically 18 processors. Run times are typically a week or more for these low *Re* cases, high *Ha* cases.

3. Results

The typical axial velocity profiles at several axial locations along the direction of flow are shown in Fig. 4. Near the onset of the expansion region, flow is pushed perpendicular to the magnetic field forming large jets near the top and bottom walls, the so-called "M-shaped" velocity profile typical of abrupt expansions or changes in magnetic field strength. The magnitude of these velocity jets deteriorates as the flow moves away from the expansion. As the flow enters the 3 parallel channels, small jets near the top and bottom walls are reformed, and then again deteriorate. Current vectors and contours of axial velocity are shown in Fig. 5a along the $y = 0$ plane (down the center of the central channel). Velocity jets and axial current loops are visible at both the abrupt expansion at $x = 50$ mm and again at the entrance to the 3 parallel channel at $x = 100$ mm. Looking more closely at the region downstream of the leading edge of the parallel channels (Fig. 5b) there appears to be several cells of current and velocity variation before the flow settles down to near fully developed flow at the exit. Similar current loops and velocity variation is seen if one looks at the center plane $y = 35$ mm of a side channel (Fig. 5c). However, the flow redevelops into classic, insulated channel, fully developed flow closer to the beginning of the parallel channel than it does in the center channel.

The flowrate in each individual channel was obtained by integrating slices of the 3D data at location $x = 110$ mm, or 10 mm downstream of the beginning of the 3 parallel channels. In all cases the middle channel received a larger share of the flow. The flow imbalances are presented in Table 3 in terms of percentage above or below uniform flow distribution. Flow imbalances as high as 26% above uniform flow in the central channel are observed. The tendency as one increases *Ha*, at fixed *Re*, is to decrease the relative imbalance. The tendency as one increases *Re*, at fixed *Ha*, is to increase the imbalance. The tendency as one increase both *Ha* and *Re* at fixed *N* is to decrease the relative imbalance. It is noted that the flow distribution in all cases with the magnetic field is more balanced than with no field at all present.

4. Discussion

The flow balance here is controlled by the MHD flow behavior in the expansion, manifold and at the transition to the parallel channels, not by any imbalance in drag in the fully developed downstream conditions such as discussed in Ref. [8]. The trend for the center channel to catch more of the flow may be partially due to the location of the supply channel directly in line with the center parallel channel, and the parabolic shape of the side-layer jet that forms at the expansion which is also centered on the central channel. A past experimental study [9] with a somewhat similar layout of parallel channels and field orientation has suggested that the flow imbalance decreases with increasing *N*, up to a certain critical *N* value beyond which there is no further change. The present data in Table 3 indicate that relative flow imbalance is decreasing with increasing *N*, whether that increase is due to increasing *Ha* or decreasing *Re*. It is possible saturation will be reached. However, a second conclusion from Ref. [9] is that the relative imbalance at a given *N* increases with increasing *Ha*. This trend is not supported by the data in Table 3, and may be due to the different orientation of the supply channel between the two studies.

A past numerical study utilizing the core flow approximation [6], again with a somewhat similar geometry to this work but with more parallel channels and electrically conducting walls between channels, also supports the trend seen in Table 3 where flowrates in the center channels are larger than the outlying channels. However,

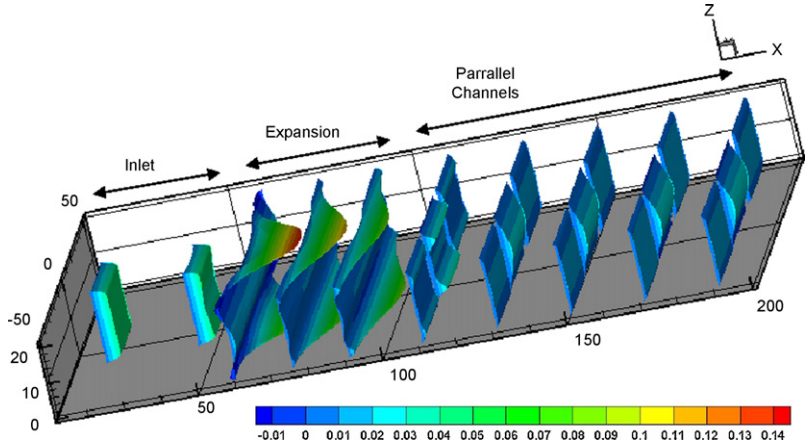

Fig. 4. Axial velocity at various axial locations (dimensions in mm, velocity in m/s).

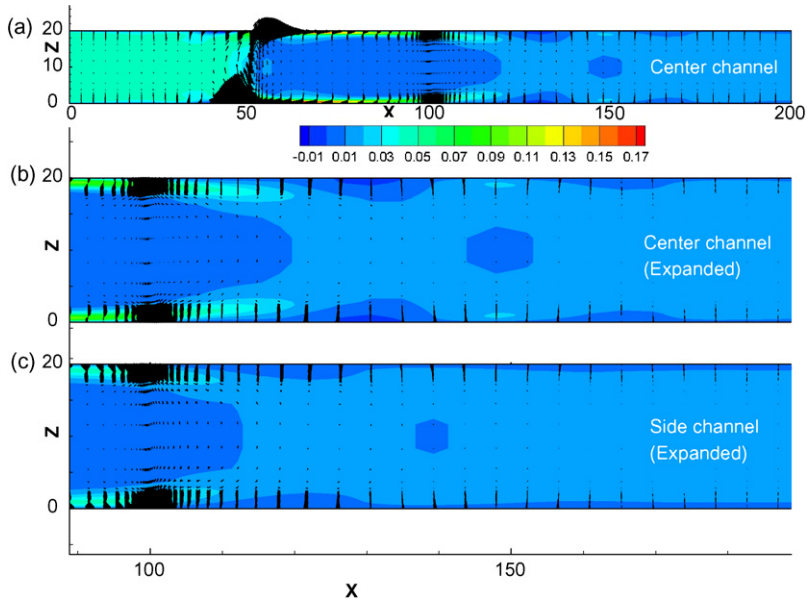

Fig. 5. Current vectors and velocity contours for case 1 as defined in Table 3: (a) $y = 0$ plane over whole axial length of the channel, (b) $y = 0$ plane expanded near the beginning of the parallel channels, and (c) $y = 35$ plane expanded near the beginning of the parallel channels (dimensions in mm, velocity in m/s).

Table 3
Percentage of flow in individual parallel channels at $x = 110$ mm, 10 mm downstream from beginning of the channels (note: 33.3% is uniform flow)

Ha	*Re*			
	250		500	
2190	Case 1: $N = 1.9 \times 10^4$	Flow, center: 41.4% Flow, side: 29.3%	$N = 9.6 \times 10^3$	Not completed
3097	Case 2: $N = 3.8 \times 10^4$	Flow, center: 37.2% Flow, side: 31.4%	Case 3: $N = 1.9 \times 10^4$	Flow, center: 38.70% Flow, side: 30.65%

the overall balance between channels was much more uniform in Ref. [6] than in the present data. It has also been proposed [10] that certain electrical coupling between channels – for instance shorting out the sidewalls near, or even within, the parallel channels – can help force more uniform flow balance between parallel channels via an MHD pumping effect. To investigate this, a simulation was performed with identical conditions to case 2 from Table 3, but with all walls in the expansion region from $x = 50$ to 100 mm treated as perfectly conducting by setting $\varphi = 0$ at the boundaries. In this simulation, flow imbalance was completely eliminated, albeit at the cost of a larger pressure drop.

5. Future work

To further investigate manifold flow and flow balancing, significant additional work is needed to clarify the many variables impacting the MHD flow:

- Using a "symmetry" boundary condition at the flow outlet may not accurately reflect the physical differences in the flow between expansion and contraction manifold regions. A preliminary flow simulation on a larger mesh explicitly modeling both expansion and contraction regions indicate that the flow distribution becomes more uniform compared with the simulations using the symmetry condition.
- The impact of a wider variety of flow conditions and geometric variations of the manifold (e.g. direction of supply channel, shape and axial length of expansion section) need to be evaluated.
- The impact of finite wall conductivity and electrical coupling between channels needs to be more fully assessed. This includes the potential to passively force a more balanced flow in channels that develop non-uniform drag characteristics, for instance due to movement or cracking of flow channel inserts.
- Comparison of full 3D simulations against both experimental data and core flow models such as in Ref. [6]. Core flow solutions can be a valuable and faster way to explore the many possible design variables. Preliminary data from the UCLA experiment indicate that flow is more balanced than these numerical simulations predict. For case 1 (again see Table 3), the experimental data indicate an almost uniform flow (35% in the central channel and 32.5% in the side channels) [11].

These additional studies are currently underway.

Acknowledgements

The authors gratefully acknowledge the support of this work by DOE Grant No. DE-FG02-86ER52123 as well as discussions, figures and information provided by K. Messadek, M. Dagher, and L. Buhler.

References

[1] C.P.C. Wong, S. Malang, M. Sawan, M. Dagher, S. Smolentsev, B. Merrill, et al., An overview of dual coolant Pb–17Li breeder first wall and blanket concept development for the US ITER-TBM design, Fusion Eng. Des. 81 (2006) 461–467.
[2] A.R. Raffray, L. El-Guebaly, S. Malang, X.R. Wang, L. Bromberg, T. Ihli, Engineering design and analysis of the ARIES-CS power plant, Fusion Sci. Tech. 54 (2008).
[3] M.J. Ni, R. Munipalli, N.B. Morley, P. Huang, M.A. Abdou, Validation case results for 2D and 3D MHD simulations, Fusion Sci. Tech. 52 (2007) 587–594.

[4] M.J. Ni, R. Munipalli, N.B. Morley, P. Huang, M.A. Abdou, A current density conservative scheme for incompressible MHD flows at a low magnetic Reynolds number. Part I. On a rectangular collocated grid system, J. Comp. Phys. 227 (2007) 174–204.
[5] M.-J. Ni, R. Munipalli, N.B. Morley, P. Huang, M.A. Abdou, A current density conservative scheme for incompressible MHD flows at a low magnetic Reynolds number. Part II. On an arbitrary collocated mesh, J. Comp. Phys. 227 (2007) 205–228.
[6] T.Q. Hua, B.F. Picolaglou, Magneto-hydrodynamic flow in a manifold and multiple rectangular coolant ducts of self-cooled blankets, Fusion Technol. 19 (1991) 102–112.
[7] L. Buhler, Inertialess magnetohydrodynamic flows in expansions and contractions, Forshungszentrum Karlsruhe Report, FZKA-6904, 2003.
[8] C. Mistrangelo, A.R. Raffray, and the ARIES Team, MHDanalysis of dual coolant Pb–17Li blanket for ARIES-CS, Fusion Sci. Tech. 52 (2007) 849–854.
[9] T.N. Aitov, A.V. Tananaev, V.A. Shinatenko, Experimental investigation of MHD flow transition to linear regime in collector mockup, Magnetohydrodynamics 3 (1989) 59–63.
[10] M.S. Tillack, N.B. Morley, Flow balancing in liquid metal blankets, Fusion Eng. Des. 27 (1995) 735–741.
[11] K. Messadek, Private communications, University of California, Los Angeles, 2007.